

Non-constant biaxial bending capacity assessment of CFST columns through interaction diagrams

Ana Espinós^{*1}, Vicente Albero², Manuel L. Romero¹,
Maximilian Mund³, Patrick Meyer³ and Peter Schaumann³

¹ Instituto de Ciencia y Tecnología del Hormigón (ICITECH), Universitat Politècnica de València, Valencia, Spain

² Department of Mechanical Engineering and Construction, Universitat Jaume I, Castellón, Spain

³ Institute for Steel Construction, Leibniz Universität Hannover, Germany

(Received March 27, 2019, Revised June 14, 2019, Accepted July 31, 2019)

Abstract. The mechanical response of concrete-filled steel tubular (CFST) columns subjected to pure compression or uniaxial bending was studied in depth over the last decades. However, the available research results on CFST columns under biaxial bending are still scarce and the lack of experimental tests for this loading situation is evident. At the same time, the design provisions in Eurocode 4 Part 1.1 for verifying the stability of CFST columns under biaxial bending make use of a simplistic interaction curve, which needs to be revised. This paper presents the outcome of a numerical investigation on slender CFST columns subjected to biaxial bending. Eccentricities differing in minor and major axis, as well as varying end moment ratios are considered in the numerical model. A parametric study is conducted for assessing the current design guidelines of EN1994-1-1. Different aspect ratios, member slenderness, reinforcement ratios and load eccentricities are studied, covering both constant and variable bending moment distribution. The numerical results are subsequently compared to the design provisions of EN1994-1-1, showing that the current interaction equation results overly conservative. An alternative interaction equation is developed by the authors, leading to a more accurate yet conservative proposal.

Keywords: biaxial bending; non-constant bending moment; concrete-filled steel tubular columns; finite element analysis; parametric studies; Eurocode 4

1. Introduction

Steel-concrete composite columns are an efficient type of members for sustaining compressive loads as compared to pure steel or reinforced concrete members. Their structural efficiency make this type of columns ideal for multi-storey or high-rise buildings where important axial loads need to be resisted with a reduced cross-section, so that the usable floor area is maximized (Han *et al.* 2014).

Extensive research has been carried out, both numerically and experimentally, to establish the load-bearing capacity of CFST columns subjected to pure compression or combined compression plus uniaxial bending (Patel *et al.* 2012a, b). In a previous investigation by Hernández-Figueirido *et al.* (2012a), an experimental campaign consisting of 36 tests on rectangular and square hollow section columns filled with normal strength concrete (NSC) and high strength concrete (HSC) was reported. The columns were subjected to a non-constant bending moment distribution with eccentricity applied about the weak axis. In a second experimental campaign (Hernández-Figueirido *et al.* 2012b), 49 tests were carried out on the same type of columns filled with HSC subjected to axial load and non-constant bending moment distribution.

According to the experimental databases by Goode and Lam (2008) and Leon *et al.* (2011), the available test data for CFST columns are mostly concentrated within the low slenderness and short effective length. In order to extend this range, 18 full-scale test were performed by Perea *et al.* (2013, 2014) with high slenderness (0.88-2.72) and high effective lengths (11-16 m). However, there is still a big gap when it comes to determine the behaviour of CFST columns under biaxial bending.

A study commissioned by the Building Research Establishment (BRE) (Anderson 1992) in the UK for assessing the design recommendations in EN 1994-1-1 (CEN 2004b) and British Standard BS 5400 for composite columns revealed that there was a large discrepancy in the predicted strengths for slender members with end moments producing other than single curvature bending (i.e., variable bending moment diagram). Due to the lack of experimental evidence, BRE carried out two series of tests: one on eight concrete-filled rectangular hollow section columns and the other on seven concrete encased columns (Wang 1999). The specimens were tested under different eccentric load positions, so that uniaxial as well as biaxial bending occurred. Based on the results of these tests, Wang (1999) assessed the design provisions in EN 1994-1-1 and BS 5400, finding that both design methods led to conservative results as compared to the test data.

A series of tests were also carried out by O'Shea and Bridge (2000) for examining the axial capacity of short

*Corresponding author, Ph.D.,
E-mail: aespinos@mes.upv.es

thin-walled steel tubes filled with high-strength concrete under combined compression and bending. The authors found that for thin-walled steel tubes filled with very high strength concrete (110 MPa), the confinement provided to the concrete core by the steel tube was negligible.

Dundar *et al.* (2008) tested a series of reinforced concrete (RC) columns under biaxial load. The experimental investigation consisted of 15 specimens (5 short square columns, 7 slender square columns and 3 L-shaped section slender columns) with different reinforcement ratios and load eccentricities. The test results were analysed in Dundar and Tokgoz (2012) with a theoretical method based on the fiber element technique. Further experimental results were published by Tokgoz and Dundar (2008), where 2 square short and 4 square slender concrete-encased composite columns plus another 4 L-shaped slender composite columns were tested. Apart from the described tests on reinforced concrete and concrete-encased composite columns, Tokgoz and Dundar (2010) performed an experimental campaign on CFST columns, consisting of 16 square biaxially loaded slender specimens. The columns were filled either with plain concrete (8 specimens) or with steel fiber reinforced concrete (8 specimens). In a later investigation by the same authors (Tokgoz *et al.* 2012), an experimental program was carried out consisting of a total of 32 biaxially loaded reinforced concrete and composite steel-concrete encased columns (4 short RC, 4 short encased, 12 slender RC and 12 slender encased columns). High strength concrete mixtures with steel fibers were used in this investigation.

Liang (2008) proposed a nonlinear analytical model for calculating the axial load-bending moment interaction diagram for short CFST columns under combined compression and biaxial bending. Nonlinear material models were used in this fiber-based model, employing an iterative process to build up the interaction curve. Through the results of the parametric study carried out by the author it was found that increasing the steel ratio or the yield strength resulted in a higher load-bearing capacity, while increasing the concrete strength decreased the so-called “C-ratio”, meaning that the column behavior was dominated by concrete. Zhao *et al.* (2009) carried out an experimental investigation on slender concrete encased composite columns. The program contained ten pin-ended columns with rectangular cross-sections subjected to uniaxial bending. In a subsequent numerical nonlinear analysis, the fiber method was used to calculate the ultimate load. Through the numerical model, it was observed that the load-bearing capacity decreased with increasing eccentricities and with higher slenderness, while the influence of the concrete strength could be neglected. Guo *et al.* (2012) reported the results of nine square and rectangular CFST columns subjected to axial load, uniaxial bending or biaxial bending. The experimental results were compared with the provisions from the AISC, EC4 and CECS design codes, showing that all of them provided safe-sided predictions.

Numerical studies have also been performed by several authors (Liang *et al.* 2012, Patel *et al.* 2015) for simulating the structural performance of biaxially loaded CFST columns. In particular, high-strength rectangular CFST

slender beam-columns were numerically simulated by Liang *et al.* (2012), accounting for progressive local buckling, initial geometric imperfections, high strength materials and second order effects. The effect of preloads arising from the upper floors of high-rise composite buildings during construction was also investigated numerically by Patel *et al.* (2014), indicating that the preloads on the steel tubes significantly reduce the stiffness and strength of CFST slender beam-columns. Other type of innovative composite columns have been recently tested under biaxial load: 26 HSC filled square steel tube columns with inner CFRP (carbon fiber-reinforced polymer) circular tube were tested by Li *et al.* (2016). The experimental results showed that the failure modes were similar to those of high strength concrete-filled steel tube columns.

In a more recent investigation, Patel *et al.* (2017) carried out an experimental campaign on rectangular CFST columns subjected to biaxial bending, with the particularity of using stainless steel at the outer section. A fiber-based model was specifically developed, with the special characteristic of the incorporation of local buckling at the steel tube, as well as the account for the strain hardening of stainless steel. The confinement of concrete was also considered in the numerical model. A parametric study was carried out for evaluating the influences of section slenderness, member slenderness, load eccentricity, load angle, steel strength and concrete strength. A simplified equation was proposed for calculating the ultimate bending moment of square concrete-filled stainless steel tubular columns.

As it has been observed in previous work by the authors (Espinós *et al.* 2018) and in the literature review performed in this section, a considerable number of investigations have been carried out on eccentrically loaded composite columns, although many of them with a different focus to the one addressed in this work (concrete encased sections, stub columns, uniaxial bending or other type of materials such as stainless steel). Therefore, the aim of this paper is to study the behaviour of slender CFST columns of rectangular section subjected to biaxial bending. For that purpose, a numerical model will be developed and validated by comparison against experimental tests. Parametric studies will be subsequently conducted in order to assess the predictions of the EN1994-1-1 (CEN 2004b) for columns subjected to combined compression and biaxial bending.

A three-dimensional $M-N$ interaction surface will be generated with the help of a Matlab computer algorithm written by the authors. The numerical database will be used to compensate the lack of experimental results in order to assess the accuracy of the 3D interaction surface.

The main contribution of this work over the existing numerical research on biaxially loaded columns is the revision of the shape of the interaction curve in EN1994-1-1 for various loading situations – i.e., different end moment ratios –. A new proposal will be presented based on the analytical method developed by the authors and evaluated through the results of the parametric studies.

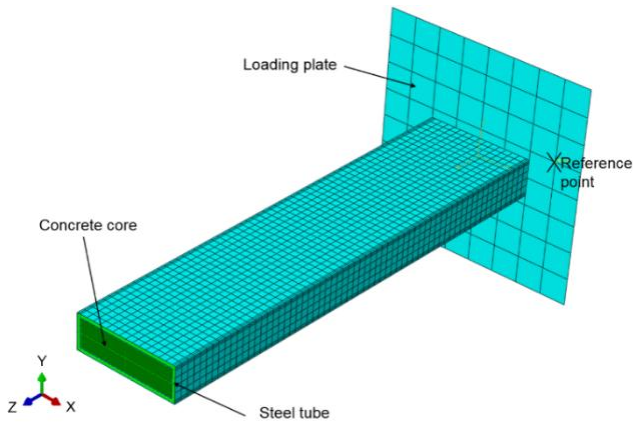


Fig. 1 Finite element mesh of a CFST column (1/2 length)

2. Finite element model

In this investigation, an advanced three-dimensional finite element model is developed through the general purpose software package ABAQUS (2014). A complete description of the numerical model is given hereafter.

2.1 Assembly and finite element mesh of the model

Four parts are assembled in order to create the numerical model of a composite steel-concrete column: two steel end plates, the outer steel tube and the concrete core. Partitions are applied into the model for controlling the finite element mesh. Two layers of finite elements are used across the thickness of the steel tube, in order to get an improved representation of the local effects, which provides similar results in the deformed shape to the alternative of meshing the steel tube with shell elements, according to the authors' experience. Based on the results of a sensitivity study, the mesh density is controlled by adopting a maximum finite element size of 2 cm, as used in previous investigations from Espinos *et al.* (2010). For meshing the steel end plates, linear four-noded shell elements with reduced integration (S4R) are used. In turn, linear eight-noded solid elements with reduced integration (C3D8R) are used for meshing the concrete core and steel tube, see Fig. 1.

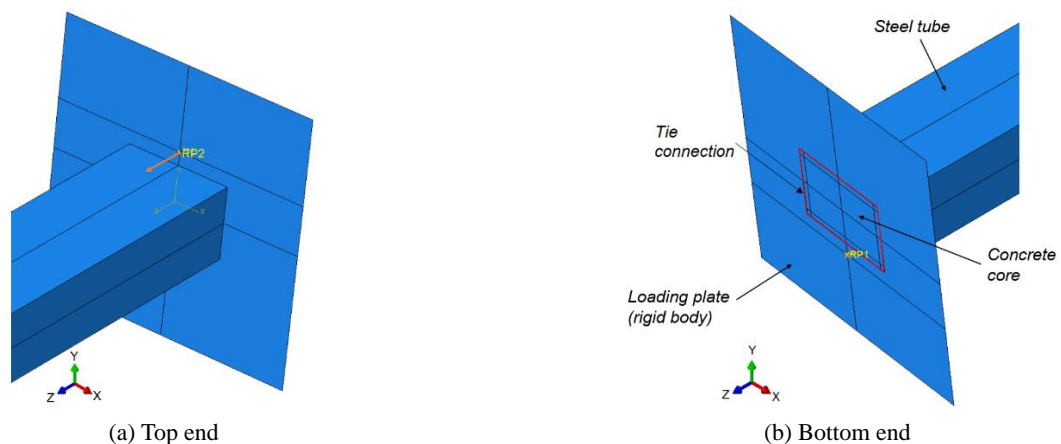


Fig. 2 Boundary conditions

2.2 Contact model at the steel-concrete interface

At the steel tube - concrete core interface, as well as at the surface between the steel end plates and the concrete core, certain contact formulations need to be defined. These contacts are modelled by means of a “surface-to-surface” interaction in ABAQUS (2014). Tangential and normal steel-concrete contact formulations are described through the interaction property. For the contact in the normal direction, the transfer of a force is only considered in compression. This is defined by means of a “hard contact” formulation with the Augmented Lagrange option. With regard to the tangent direction, the Coulomb friction model is employed, making use of a friction coefficient μ of 0.3, according to a previous sensitivity study. The values assumed for the contact properties are obtained from previous calibrations of the model performed by the authors (Espinos *et al.* 2010).

2.3 Application of the boundary conditions

Steel plates are modelled at both ends of the column as rigid bodies in order to apply the required boundary conditions. These rigid bodies behave in such a way that the movements of all their nodes are coupled to those of a reference point. The position of the reference points are varied according to the load eccentricity – i.e. point of load application –.

The top end reference point is free to move axially and rotate (Fig. 2(a)), while at the bottom end reference point no displacements are permitted, being the rotation allowed (Fig. 2(b)). In order to reproduce the load application, a displacement is imposed at the top end reference point.

2.4 Initial geometry and imperfection of the column

An initial geometrical imperfection is taken into account in the modelling of the columns. In order to do so, an eigenmode analysis is previously carried out and the deformed shape of the selected buckling mode is subsequently imported into the mechanical model as the starting geometry. From the previous eigenmode analysis, either the first buckling mode shape (bending about the

weak axis) or the second buckling mode shape (bending about the strong axis) is selected depending on the expected failure axis in the test. In particular, for uniaxially loaded columns with minor axis eccentricity as well as for biaxially loaded columns, the first buckling mode is used, while for uniaxially loaded columns with major axis eccentricity, the second buckling mode is selected.

The initial imperfection of the column obtained in this way is then imported into the mechanical model and amplified at mid-height by a factor of $L/1000$, as previously used by other authors (Tokgoz *et al.* 2012, Patel *et al.* 2017) for modelling concrete-filled steel tubular columns and confirmed from the results of a sensitivity study by the own authors.

2.5 Material constitutive models for steel and concrete

The mechanical behaviour of steel is represented through an isotropic elastic-plastic model based on the constitutive model from EN1993-1-1 (CEN 2005). The elastic part is defined by means of two parameters: The Young's modulus (E) and the Poisson's ratio (ν), taken as 0.3. For the characterization of the plastic behaviour of steel, plastic strains are defined together with the yield stress.

For describing the uniaxial stress-strain relation of concrete in compression, the simplified model from EN 1992-1-1 (CEN 2004a) with a linear descending branch is used. The values of the ultimate strain and the strain at reaching the maximum strength are obtained from Table 3.1 in EN 1992-1-1 (CEN 2004a). The Poisson's ratio is assumed to be equal to 0.2 for uncracked concrete as per Clause 3.1.3 (4) in the same code. For characterizing the plastic behaviour, the Concrete Damaged Plasticity (CDP) model available in the ABAQUS (2014) library is used. The input parameters for the concrete plasticity model are obtained from previous research by the authors (Albero *et al.* 2016) and summarized in Table 1.

Based on previous studies on the confinement effect conducted by Liang (2015), it can be confirmed that the confinement effect in rectangular CFST stub columns only influences the ductility of the concrete core, but it does not increase its compressive strength, as it is the case for circular CFST columns. Moreover, Liang (2015) showed that in slender CFST columns, the concrete confinement effect decreases with an increase in the column slenderness or the loading eccentricity. For all these reasons, the confinement effect has been ignored in the material constitutive model for concrete.

The behaviour of concrete in tension is described through a simplified bi-linear stress-strain relation. In the absence of any specific indication for the value of the ultimate tensile strain in the Eurocode, it is assumed as four times the value of the strain at peak stress, following the

Table 1 Parameters for CDP model

Dilation angle	Eccentricity	f_{b0}/f_{c0}	K	Viscosity parameter
15	0.1	1.16	2/3	0

recommendation from the CEB-FIB Model Code2010 (FIB 2010).

3. Validation of the numerical model

In this section, the developed numerical model is validated by comparison with experimental test results from the literature. In particular, two series of uniaxially loaded column tests reported by Hernández-Figueirido *et al.* (2012a) and Matsui *et al.* (1995) are used for validation, as well as a series of biaxially loaded columns from an experimental campaign performed by Wang (1999). These tests are suitable for validating the numerical model, since the test setup and type of section is coincident with the one analysed in this research. Other experimental programs existing in the literature and described in Section 1 do not fit exactly to the problem addressed in this paper, due to the difference on the materials used – i.e., high strength steel, high strength concrete, stainless steel – type of section or loading conditions, so they were discarded. The selected columns cover a wide range of aspect ratios, column slenderness, B/t ratios, relative eccentricities and end moment ratios, in order to guarantee the reliability of the validation.

On a first instance, the numerical model is validated for uniaxial bending by comparison with test results from the experimental campaign carried out by Hernández-Figueirido *et al.* (2012a), where a series of rectangular CFST columns were tested uniaxially under unequal load eccentricities (end moment ratio of 1 and 0). A total of nine columns with three different cross-sections and three different load situations are used for validation, as listed in Table 2. The nominal cylinder strength was 30 MPa and the steel grade S275JR, although the real strengths measured by coupon tests were used in the numerical simulations.

The last three columns in Table 2 show the comparison between numerical and test results for all the column compared in this series, as well as the prediction error. It can be seen that the numerical model is in good agreement with the experimental results, with an average error of

Table 2 Summary of test data from Hernández-Figueirido *et al.* (2012a)

Test no.	B (mm)	H (mm)	t (mm)	e^{top} (mm)	e^{bot} (mm)	F_{EXP} (kN)	F_{NUM} (kN)	F_{EXP}/F_{NUM}
2	100	100	4	20	20	380.8	398.5	0.96
4	150	100	4	20	20	535.8	532	1.01
6	150	100	5	20	20	605.6	654.2	0.93
8	100	100	4	50	50	244	271.8	0.90
10	150	100	4	50	50	356	382.4	0.93
12	150	100	5	50	50	395	442.9	0.89
26	100	100	4	20	0	474.7	538	0.88
28	150	100	4	20	0	624.4	630.6	0.99
30	150	100	5	20	0	728.5	756.4	0.96
Avg.								0.94
Std. dev.								0.04

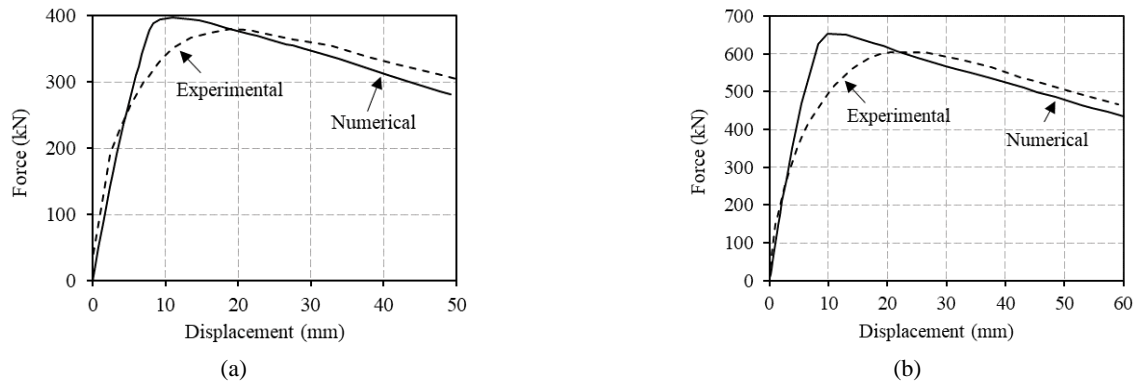


Fig. 3 Comparison between numerical and experimental force-displacement curves for test No. 2 (a) and No. 6 (b) from Hernández-Figueirido *et al.* (2012a)

0.94 and a reduced dispersion of results.

Fig. 3 shows the comparison between the experimental and numerical force-displacement curves for specimens No. 2 and 6 from Hernández-Figueirido *et al.* (2012a). The initial stiffness is in a good agreement; however the elastic branch results longer in the numerical model than in the tests, being these differences related to the forming process of the tested columns, which were cold formed.

In order to extend the validation, a series of tests on square CFST columns subjected to uniaxial bending from an experimental investigation by Matsui *et al.* (1995) are selected, as previously employed by Patel *et al.* (2012a). The columns had a square cross-section of 149.8 mm width and 4.27 mm wall thickness. Steel tubes with yield strength of 445 MPa were filled with normal strength concrete of 31.9 MPa. The eccentricity of the applied axial load varied from zero to a maximum of 125 mm. Nine of the columns were selected to be used in the validation, with a varying length ranging from 2700 mm to 4500 mm, thus covering a wide range of column slenderness. Fig. 4 shows the results of one specimen from these test series used for validation. Although the ultimate load is slightly overpredicted in this case, the overall force-displacement curve is well captured and the stiffness is in good agreement for both elastic and plastic range, which is a trend observed for all the columns.

On a second instance, the numerical model is validated for biaxial bending by comparison with test results from the experimental campaign performed by Wang (1999).

Wang (1999) carried out two sets of experimental tests on steel-concrete composite slender columns: eight of them being concrete-filled RHS sections and other group of eight corresponding to concrete encased columns. In particular, the first group is considered in this work. The experimental campaign carried out by Wang comprised 2 columns with minor axis eccentricity, 2 with major axis eccentricity and 4 columns under biaxial bending. Different end moment ratios ($r = e^{\text{bottom}}/e^{\text{top}}$) were also applied in the tests so as to obtain different bending moment distributions, either $r = 0$ (eccentricity only at top end) or $r = -1$ (top and bottom end eccentricity with inverted directions). The main characteristics of these tests are summarized in Table 3, where the values of the applied eccentricity and end moment ratio are given for both axes.

Note that specimen RHS8 was excluded from the test

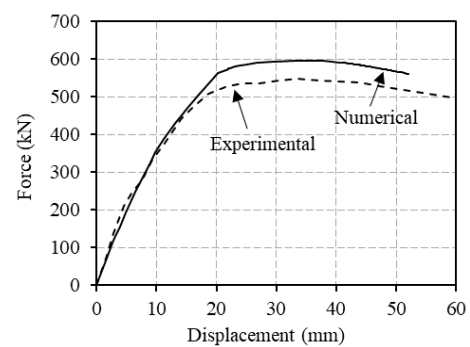


Fig. 4 Comparison between numerical and experimental force-displacement curves for test No. S3 from Matsui *et al.* (1995)

Table 3 Summary of test data from Wang (1999)

Test no.	Major axis		Minor axis		Ultimate load		$F_{\text{EXP}}/F_{\text{NUM}}$
	e_z (mm)	r_y	e_y (mm)	r_z	F_{EXP} (kN)	F_{NUM} (kN)	
RHS1	0	-	55	-1	368	315.2	1.17
RHS2	0	-	55	0	246	236	1.04
RHS3	55	0	110	0	172	172.5	1.00
RHS4	55	0	110	-1	238	234.4	1.02
RHS5	55	-1	110	-1	251	231.8	1.08
RHS6	55	0	55	0	234	225	1.04
RHS7	55	-1	0	-	520	499.6	1.04
Avg.							1.06
Std. dev.							0.06

database due to an unexpected failure behaviour in the test as reported by Wang (1999).

The column dimensions and materials were the same for all the specimens. The length of all the tested specimens was 4 meters. The RHS sections were hot-rolled, being their dimensions 120 mm × 80 mm × 6.3 mm and filled with plain concrete. The relative slenderness of the columns was 1.10 in major axis direction and 1.56 for the minor axis. The nominal material properties were: $f_c = 50 \text{ N/mm}^2$, $E = 37000 \text{ N/mm}^2$ and $f_y = 370 \text{ N/mm}^2$.

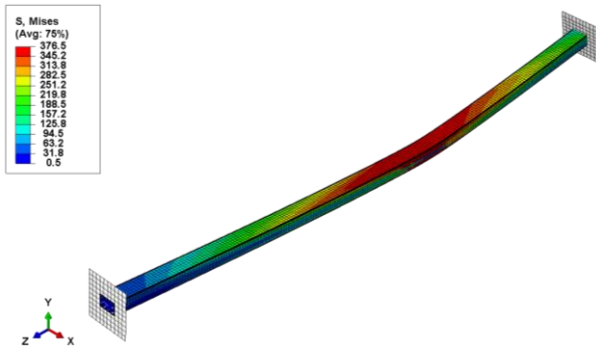
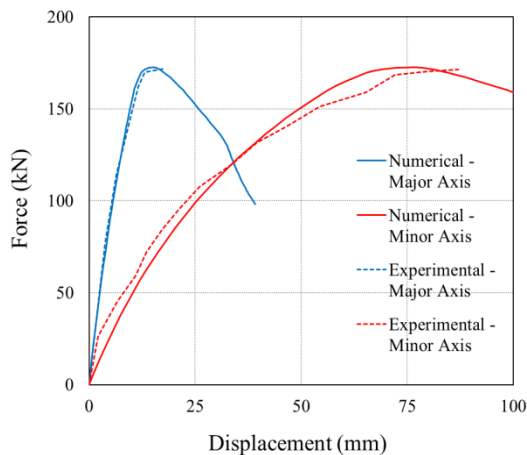
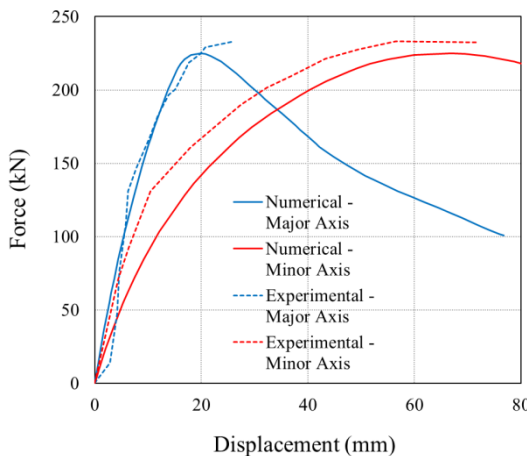


Fig. 5 Von Mises stress 3D plot, for column RHS3 from Wang (1999)



(a)



(b)

Fig. 6 Comparison between numerical and experimental force-displacement curves for columns RHS3 (a) and RHS6 (b) from Wang (1999)

The listed columns were simulated with the previously described numerical model. The deformed shape of one of the columns (RHS3) after analysis can be seen in Fig. 5, together with the von Mises stress field.

Table 3 presents the results of the validation by comparison between the numerical simulations and test results from Wang (1999). It can be seen that the model

delivers results which are in good agreement with the experimental data. The scatter of the predictions is low, with most of the calculations laying on the safe side.

The force versus displacement curves are used for comparison between the numerical model and the test results, with especial account to the ultimate load and stiffness. Fig. 6 shows the comparison between the experimental and numerical force-displacement curves for specimens RHS3 and RHS6, with simultaneous minor and major axis eccentricity – i.e., biaxially loaded –. Solid lines represent the numerical results, while the experimentally measured data are represented with dashed lines. Red lines show the minor axis displacement, while major axis displacement is represented with blue lines. It can be observed that the numerical model is able to capture the overall behaviour of the columns, representing with good accuracy the ultimate load and the corresponding displacement at peak load. The initial stiffness is also in good agreement with the tests.

In order to get an overview of all the validation process, Fig. 7 summarizes the results of all the case specimens, where a comparison between the calculated and measured ultimate loads is presented for the three test series used for validation. From this figure, it can be inferred that the numerical model can predict the behaviour of both uniaxially and biaxially loaded rectangular CFST columns with good accuracy, with most of the predictions lying within the $\pm 10\%$ region. The average prediction error is 0.95, with a reduced dispersion of results (0.09 standard deviation).

4. Parametric studies

The previously validated numerical model was used to conduct a comprehensive parametric study on concrete-filled RHS columns subjected to biaxial bending, with the aim of generating a numerical database that serves as a basis for the assessment of the current design guidelines of EN1994-1-1 (CEN 2004b), as well as for studying the

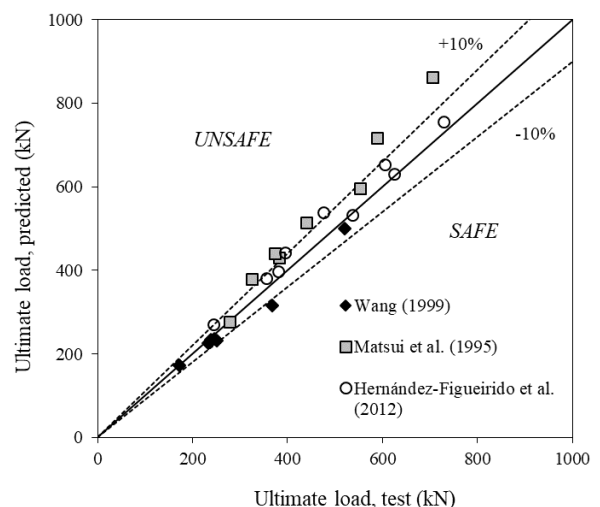


Fig. 7 Comparison between experimental and numerical ultimate loads

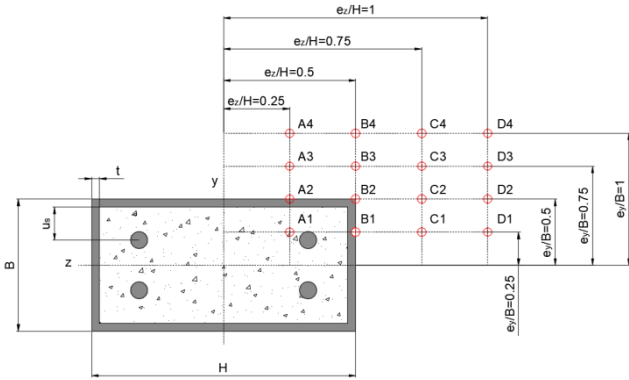


Fig. 8 Points of load application considered in the parametric studies

influence of the different parameters over the composite column capacity under biaxial bending.

4.1 Definition of analysis cases

Three cross-sections were used, with three different aspect ratios (H/B): 1, 2 and 3. Five slenderness were studied, by increasing the L/B ratio from 10 to 30. Some of the columns were reinforced, with reinforcement ratios of

Table 4 Combinations of analysis cases for the parametric studies

Parameter	Values				
Aspect ratio (H/B)	1	2	3		
$H \times B$ (mm)	100 × 100	200 × 100	300 × 100		
t (mm)	5	6	10		
B/t	20	16.6	10		
L (mm)	1000	1500	2000	2500	3000
L/B	10	15	20	25	30
Reinforcement	4φ8 mm (2.48%)	4φ16 mm (4.86%)	4φ16 mm (4.86%)	0	0
u_s (mm)		30			-
e_y/B		0.25 / 0.5 / 0.75 / 1			
e_z/H		0.25 / 0.5 / 0.75 / 1			
$r = e^{bottom} / e^{top}$		1 / 0 / -1			

2.48% and 4.86%. For each geometry, four relative eccentricities about minor axis (e_y/B) and major axis (e_z/H) were used, generating for each column specimen 16 different loading scenarios (see Fig. 8). Regarding the end moment ratio, three different values were analysed (Fig. 9),

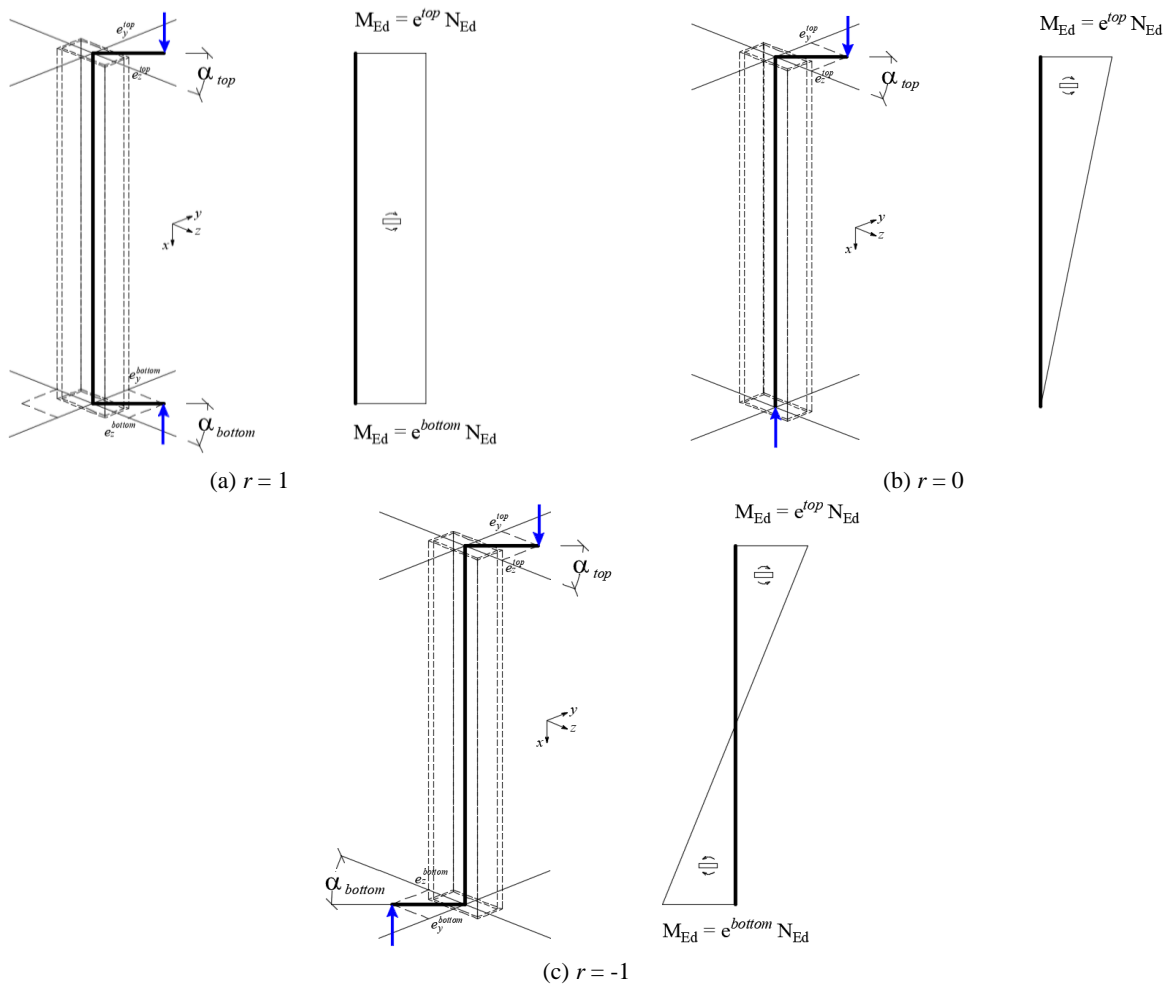


Fig. 9 Different end moment ratios studied

covering both constant and variable bending moment distributions ($r = e^{\text{bottom}}/e^{\text{top}} = 1, 0$ and -1). Table 4 shows the range of variation of the studied parameters, resulting a total of 240 analysis cases, by combining the different parameters described.

Similarly to Leite *et al.* (2014), the skew angle (α) is defined as the angle between the relative eccentricities applied at both axes, as given in Eq. (1) and Fig. 9.

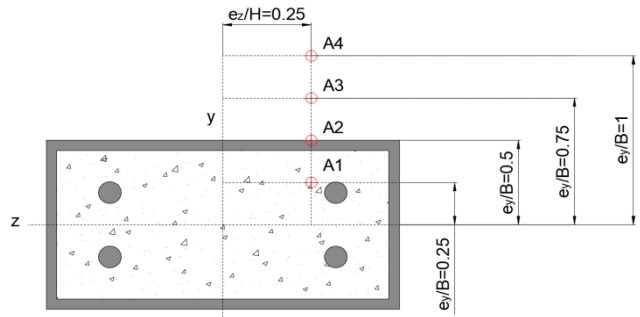
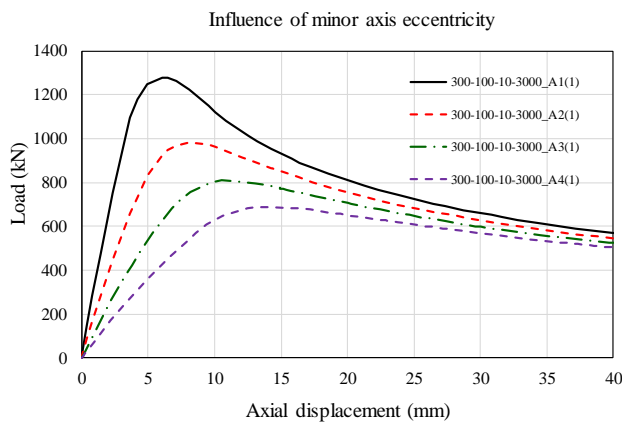
$$\alpha = \arctg \frac{e_y / B}{e_z / H} \quad (1)$$

It is worth noting that in this investigation the skew angle at top and bottom end of the column is kept equal, i.e., $\alpha_{\text{top}} = \alpha_{\text{bottom}}$.

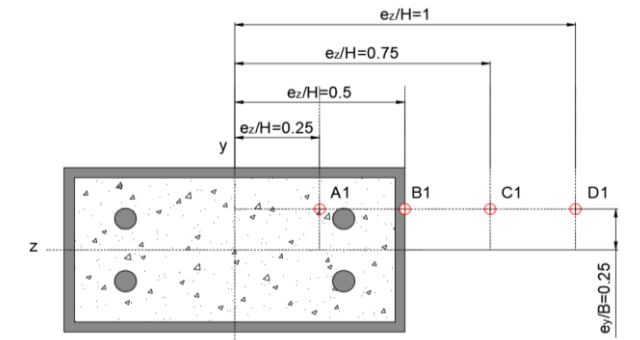
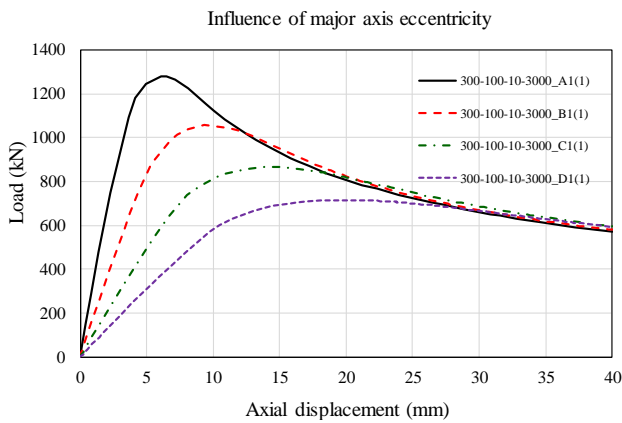
The rest of the input parameters adopted in the parametric studies were constant for all the columns analysed: hinged boundary conditions, steel tube yield strength $f_y = 355$ MPa, concrete compressive strength $f_c = 30$ MPa and reinforcing bars yield strength $f_s = 500$ MPa.

4.2 Analysis of results

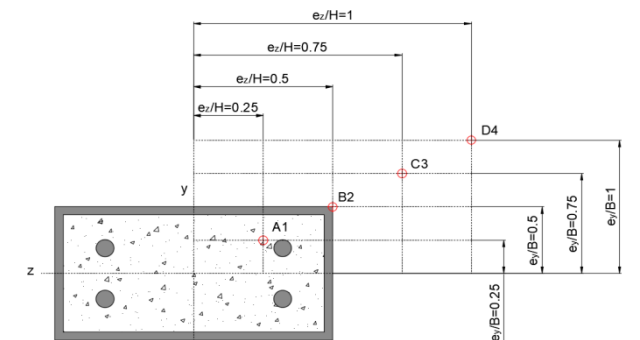
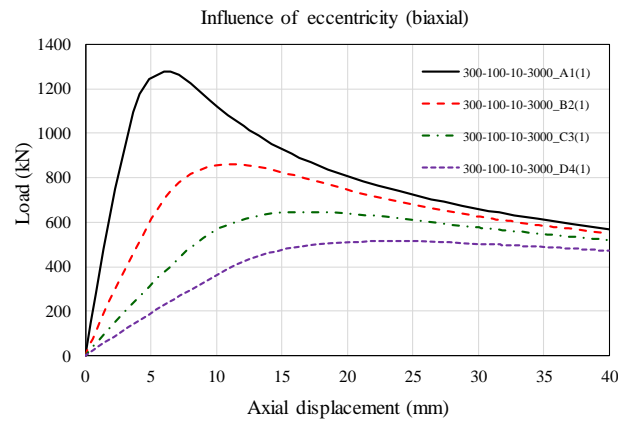
The results of the parametric studies are evaluated in



(a)



(b)



(c)

Fig. 10 Influence of load eccentricity, for column series 300-100-10-3000: (a) Minor axis eccentricity; (b) Major axis eccentricity; (c) Equal relative eccentricity at both axes

this section. For each case analysis, the axial force versus displacement curve is obtained. The influence of the following parameters is investigated: minor and major axis eccentricity, end moment ratio and member slenderness.

The notation used for codifying the column specimens in the figures is as follows: $H(\text{mm}) - B(\text{mm}) - t(\text{mm}) - L(\text{mm})$ (i.e., 300-100-10-3000).

Fig. 10 shows the influence of the load eccentricity, for column series 300-100-10-3000. In Fig. 8(a) the eccentricity is varied along the y-axis from position A1 to A4, in Fig. 8(b) it is varied along the z-axis from position A1 to D1 and finally in Fig. 8c the relative eccentricity applied at both axes is equal, i.e., position A1 to D4. As it can be seen, when the eccentricity about the minor axis is increased (A1 to A4), the ultimate load decreases. The same effect occurs for eccentricity about the major axis (A1 to D1) and for equal relative eccentricities (A1 to D4). The reduction of the column capacity is more evident for the latter case, as it can be seen in the dramatic reduction of the stiffness and ultimate load as the eccentricity increases.

Fig. 11 shows the influence of the end moment ratio, for column series 100-100-5-1000 and different positions of the load: A1, B2, C3 and D4. For all the loading positions compared, the ultimate load is higher for the case with end moment ratio $r = -1$, while the lower load is obtained under $r = 1$. The reason is that for constant bending moment ($r = 1$) the maximum bending moment is located at mid-height of the column, where the first order bending moment and

the moment from imperfection are superimposed, giving a higher maximum value than for variable bending moment, where the maximum bending moment is located either at the column ends ($r = -1$) – where no moment from imperfection occurs – or between the column end and mid-section ($r = 0$), with a lower maximum value. It can be also noticed that for $r = 0$ and $r = -1$ the slope of the ascending branch is steeper than for $r = 1$, meaning that the column behaves in a stiffer manner for these end moment distributions.

This is due to the curvature of the column caused by the moment distribution: single curvature bending for $r = 1$ with maximum displacement at mid-height versus double curvature bending for $r = -1$ with no transversal displacement at mid-height.

Therefore, the situation with variable bending moment results more favourable for the column than applying a constant bending moment, as in the first case the end moments applied in opposite directions compensate with each other, resulting in a higher stability for the column.

Fig. 12 shows the influence of member slenderness for column series 300-100-10, for different positions of the load: A1 and D4, D1 and D4, A2 and D2, A3 and D3. Each pair of curves represent the same load position and end moment distribution ($r = 1$) for columns with equal section and different length – i.e., different slenderness –. It can be seen that in all the combinations studied, the column with higher length and therefore higher member slenderness (3 m

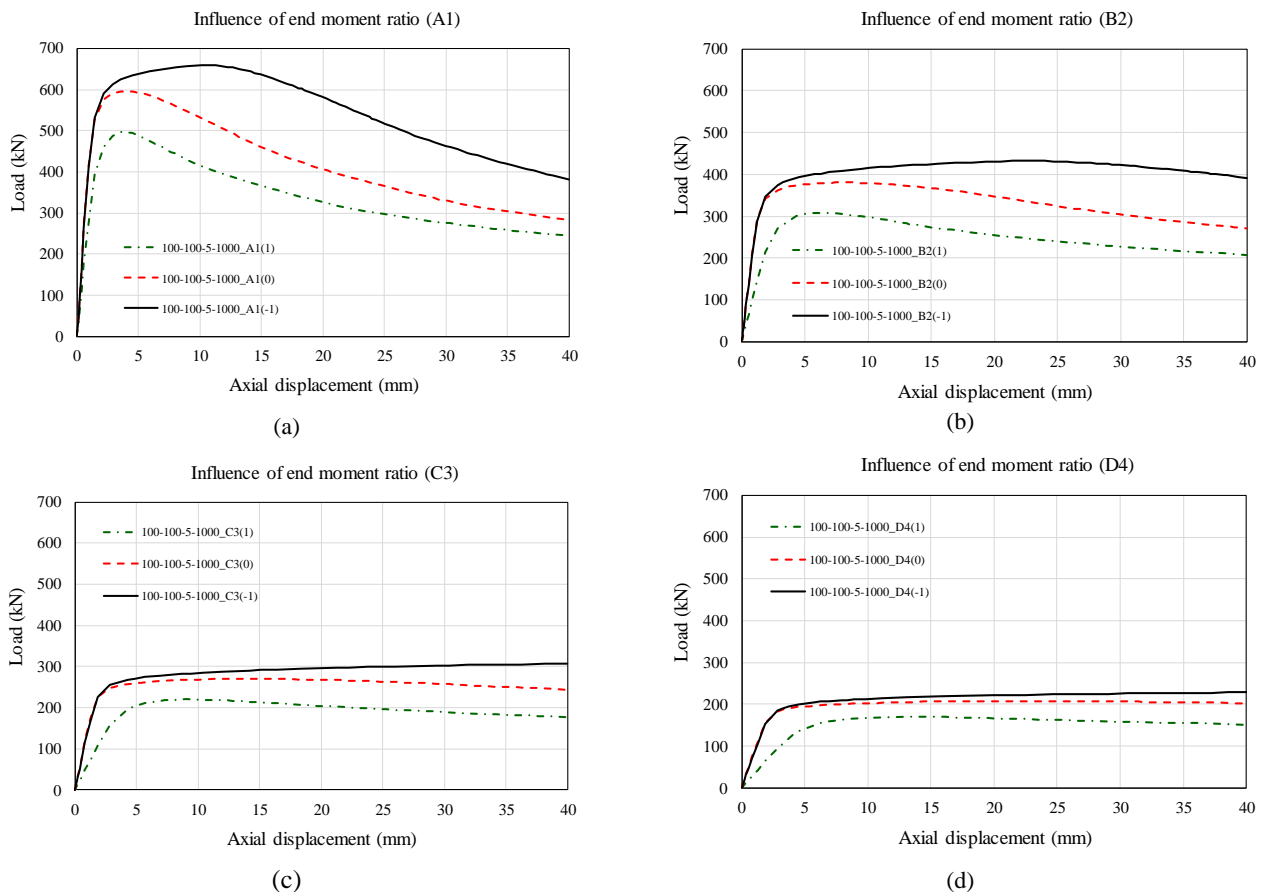


Fig. 11 Influence of end moment ratio, for column series 100-100-5-1000: (a) A1; (b) B2; (c) C3; (d) D4

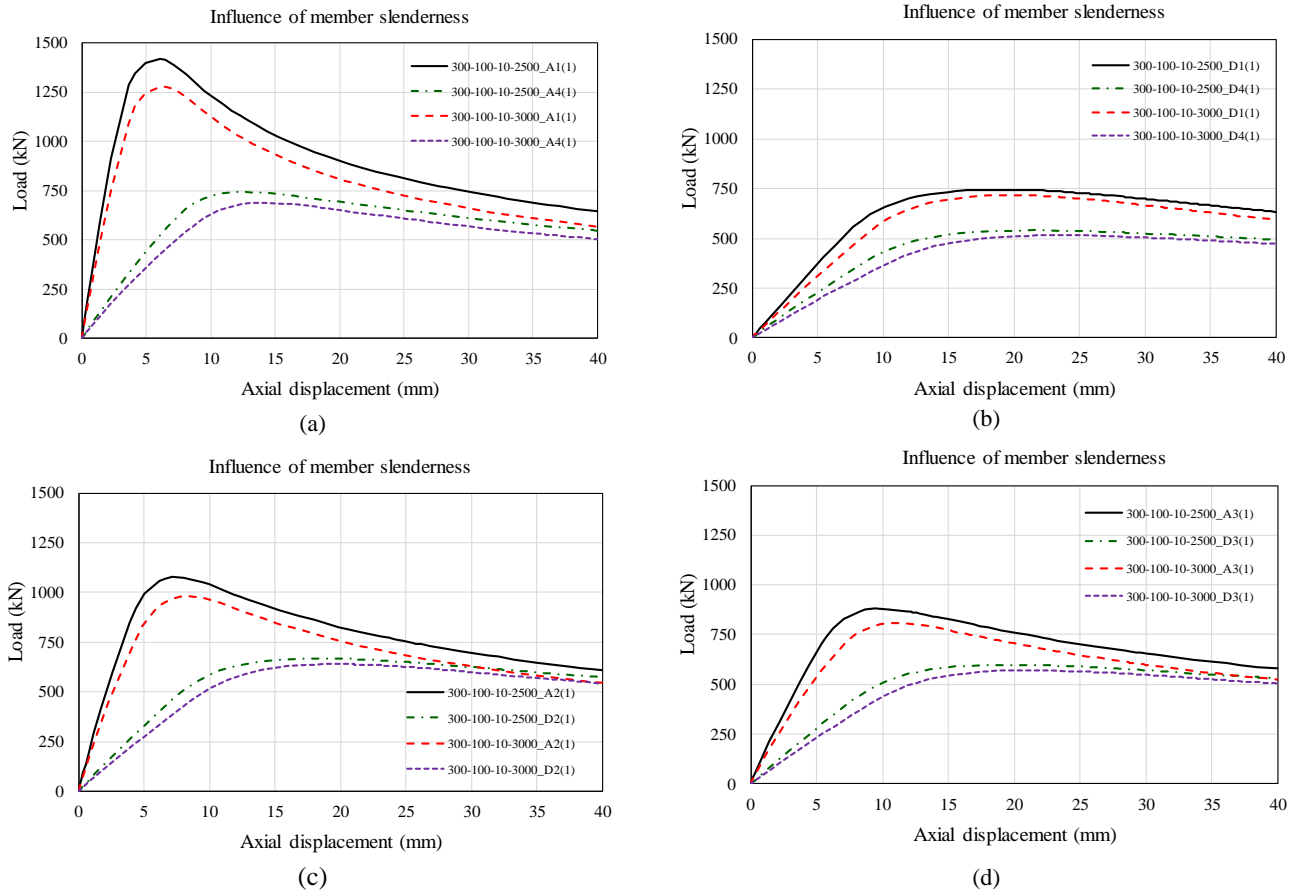


Fig. 12 Influence of member slenderness, for column series 300-100-10: (a) A1-A4; (b) D1-D4; (c) A2-D2; (d) A3-D3

versus 2.5 m) has a lower ultimate load, therefore these results confirm that as the column slenderness increases, the capacity of the column decreases, regardless the direction of the load applied. It can be also seen that the effect is similar for increasing eccentricities and for both axes: increasing minor axis bending (A1 versus A4, D1 versus D4) and increasing major axis bending (A2 versus D2, A3 versus D3). The magnitude of the reduction with the slenderness is similar in all cases.

5. Assessment of the current design guidelines in EN1994-1-1

The results of the parametric studies are used in this section to evaluate the accuracy of the calculation method in Clause 6.7.3.7 of EN1994-1-1 (CEN 2004b) for members in combined compression and biaxial bending.

5.1 Cross-sectional calculation

For combined compression and biaxial bending, Clause 6.7.3.7 of EN1994-1-1 makes use the well-known Bresler's equation (Bresler 1960), with exponents equal to one (i.e., straight line).

The numerators in Eq. (2) are the applied bending moments about each section axis. The denominators are the plastic bending resistances taking into account the axial

force, which may be obtained by intersecting the uniaxial interaction diagrams at the corresponding axial load level.

$$\frac{M_{y,Ed}}{M_{pl,y,N,Rd}} + \frac{M_{z,Ed}}{M_{pl,z,N,Rd}} \leq 1,0 \quad (2)$$

Let "a" and "b" be the exponents in the original Bresler's equation

$$\left(\frac{M_{y,Ed}}{M_{pl,y,N,Rd}} \right)^a + \left(\frac{M_{z,Ed}}{M_{pl,z,N,Rd}} \right)^b \leq 1,0 \quad (3)$$

For pure steel or concrete columns, the corresponding European standards present similar equations with exponents "a" and "b" different to unity. For steel sections, EN1993-1-1 (CEN 2005) in its Clause 6.2.9.1(6) establishes different exponents in Eq. (3) depending on the cross-section shape and the ratio between the applied axial load and ultimate plastic load, in particular for rectangular hollow sections

$$a = b = \frac{1,66}{1 - 1,13n^2} \quad \text{but } a, b \leq 6 \quad (4)$$

where $n = N_{Ed}/N_{pl,Rd}$

In turn, for concrete sections, EN1992-1-1 (CEN

Table 5 Values of exponents “a” and “b” as per Clause 5.8.9(4) in EN 1992-1-1 (CEN 2004a)

$n = N_{Ed}/N_{pl,Rd}$	0.1	0.7	1.0
a, b	1	1.5	2

2004a) in its Clause 5.8.9(4) defines exponents “a” and “b” for rectangular cross-sections between 1 and 2 in function of the ratio between the applied axial load and ultimate plastic load, as given in Table 5. For intermediate values, linear interpolation can be applied.

As a first stage of verification of the current method in Eurocode 4, the shape of this interaction surface is revised hereafter.

With the help of a computer code developed by the authors in the software tool Matlab (MathWorks 2016), the $M_y - M_z$ interaction curve is theoretically calculated for the different cross-sections studied in the parametric studies and afterwards compared with the different interaction curve shapes proposed by Eurocodes 2, 3 and 4.

For each load level (i.e., same applied axial load N_{Ed}), the developed algorithm allows building up the failure surface. The procedure for plotting these curves is described hereafter.

First, the cross-section is integrated by using a cell decomposition method through the Matlab mesh tool, Fig. 13. The strain field along the cross-section is computed in each cell centroid by assuming a linear strain distribution - i.e., plain sections remain plane after bending -, see Fig. 13, and the curvature (κ) of the cross-section is derived through this linear distribution.

Next, the corresponding stress for each cell can be obtained from its corresponding stress-strain curve, depending on its material (steel, concrete or reinforcing bars). The material nonlinearities are taken into account in the code. The constitutive models from EN1993-1-1 (CEN 2005) for steel and EN1992-1-1 (CEN 2004a) for concrete, respectively, were adopted for this purpose.

Once the stresses of all cells are known, an iterative process is applied to obtain the plastic neutral axis location through the force equilibrium condition. The applied

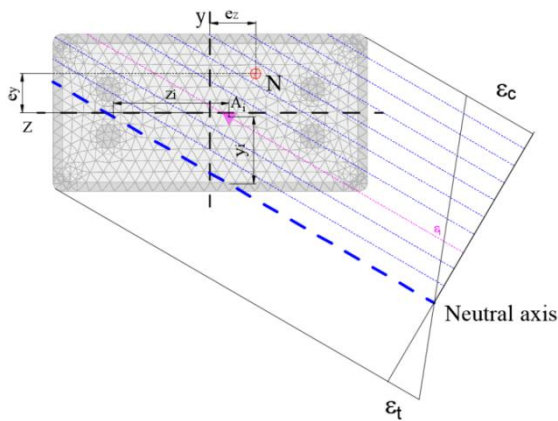


Fig. 13 Discretization of the CFST cross-section and strain distribution

axial load (N_{Ed}) must be also taken into account in this equilibrium.

$$\sum_{i=1}^n A_i \sigma_i - N_{Ed} = 0 \tag{5}$$

Then, the bending moment equilibrium conditions are used to compute the resisted bending moments about each direction, corresponding to the given axial load ($M_{pl,y,N,Rd}$, $M_{pl,z,N,Rd}$).

$$\sum_{i=1}^n A_i \sigma_i y_i - M_{pl,z,N,Rd} = 0 \tag{6}$$

$$\sum_{i=1}^n A_i \sigma_i z_i - M_{pl,y,N,Rd} = 0 \tag{7}$$

This procedure is computed repeatedly by increasing the cross-section curvature (κ) to obtain the $M-\kappa$ curve. The plastic bending resistance of the cross-section is defined as the maximum moment value achieved in the $M-\kappa$ curve.

Additionally, the process described above is also repeated by rotating the neutral axis and increasing the applied axial load (N_{Ed}) from 0 to the value of the cross-section plastic resistance ($N_{pl,Rd}$), in order to create the whole interaction surface, see Fig. 14.

Fig. 15 shows the results of applying the developed algorithm for the three cross-sections studied. Due to their double symmetry, only a quarter of the interaction surface is plotted. For each section, four different load levels ($n = N_{Ed}/N_{pl,Rd}$) have been studied (0, 0.25, 0.5 and 0.75). At each load level, six evenly distributed plastic neutral axis directions with angles between 0 and 90° are calculated (every 15°). The calculated points are afterwards interpolated by the blue line, and this curve is compared with the one from Eurocode 2 (dashed-pink) and Eurocode 3 (dashed-green). It can be seen that the analytical curve

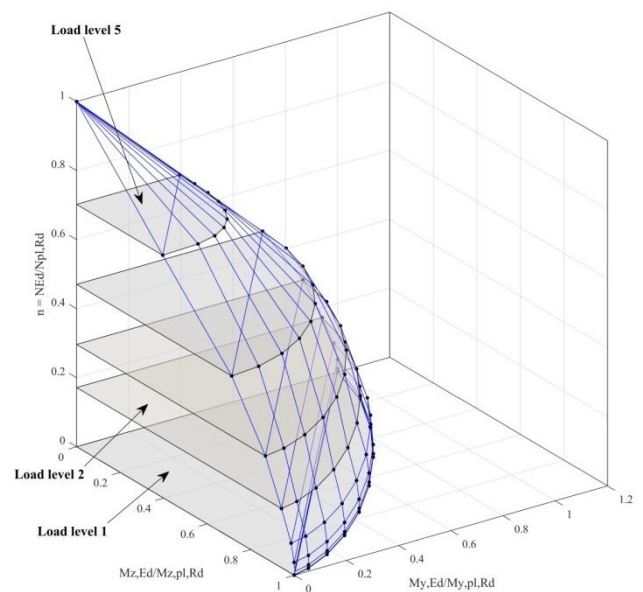


Fig. 14 Construction of the 3D interaction surface from the interaction curves at different load levels

lies between those of EC2 (conservative) and EC3 (unconservative). Obviously, the straight line given in EC4 results in safe-sided predictions, which do not follow the shape of the real failure surface.

In view of these results, it can be thought that if exponents “a” and “b” higher than one and with values comprised between those proposed by EC2 and EC3 are used for composite columns, a better fit to the data may be obtained. A similar shape to that from Eq. (4) is proposed. The coefficients in this equation are adjusted by means of a function for minimizing the error, which is measured as the area between the red curves in the right-hand side plots of

Fig. 15 (proposal) and the blue curves (numerical results). The adjusted expression that minimizes the error results as follows

$$a = b = \frac{1,42}{1-1,17n^2} \text{ but } a, b \leq 3 \quad (8)$$

As shown in Fig. 15 (right), this proposal still results conservative, while providing a better fit to the numerical data than the assumption of EN1994-1-1 of a straight line. Also, it results compact and easy to apply, and - as one would expect - lies between the curves from the respective Eurocodes for steel (EC3) and concrete (EC2).

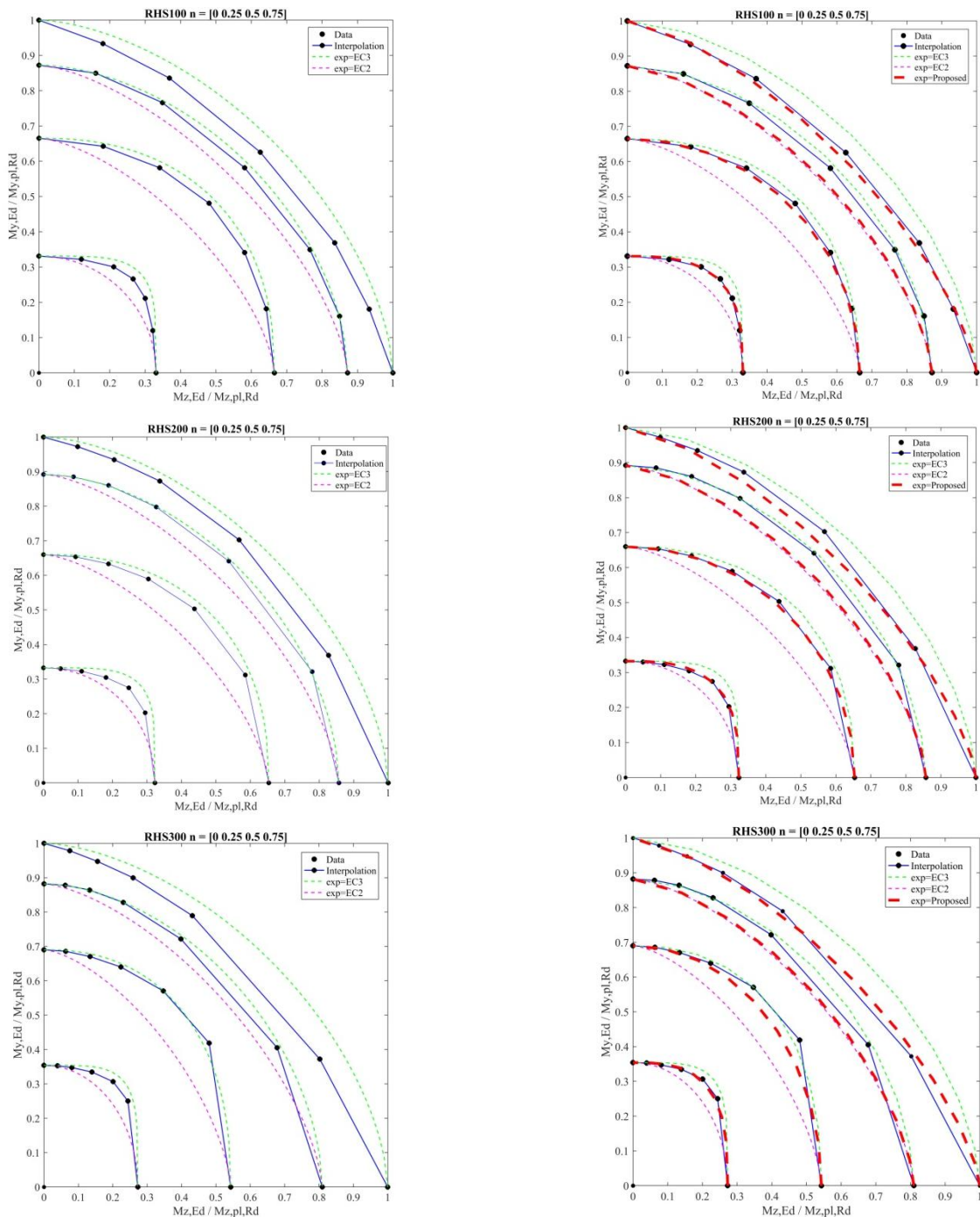


Fig. 15 Comparison of My-Mz interaction curves (left) and proposed equation (right)

5.1 Member calculation

In order to evaluate the predictions of Eurocode 4 for slender members subjected to biaxial bending, the numerical results from the parametric studies carried out in Section 4 are used in this section, so that the second order effects are now taken into account. For each of the columns analysed, the axial load value N_{Ed} is obtained from the numerical simulation, and through this load value, the applied bending moments on both axes are computed by using the corresponding eccentricities and imperfection.

The numerically obtained axial load N_{Ed} is multiplied by the eccentricity applied on each axis (e_z or e_y) and a moment magnification factor (k) for taking into account the second order effects. Therefore, the bending moments about major and minor axis, are respectively

$$M_{y,Ed}(x) = N_{Ed}e_zk \left[(r - 1) \frac{x}{L} + 1 \right] \quad (9)$$

$$M_{z,Ed}(x) = N_{Ed}e_yk \left[(r - 1) \frac{x}{L} + 1 \right] \quad (10)$$

where $r = e^{\text{bottom}}/e^{\text{top}}$ is the end moment ratio;
 e_z is the major axis eccentricity;
 e_y is the minor axis eccentricity.

Note that these equations are valid for all the loading combinations used in the parametric studies, with $r = 1, 0$ or -1 , giving the moment as a function of coordinate 'x' along the column.

The k factors are calculated as given in Clause 6.7.3.4(5) of EN1994-1-1 (CEN 2004b)

$$k = \frac{\beta}{1 - \frac{N_{Ed}}{N_{cr,eff}}} \quad (11)$$

where β is an equivalent moment factor given in Table 6.4 of EN1994-1-1, as a function of the end moment ratio (r) and bending moment distribution (either linear or parabolic). For a linear distribution of moments, which is the case for the three end moment ratios considered in the parametric studies ($r = 1, 0, -1$)

$$\beta = 0.66 + 0.44r \quad \text{but } \beta \geq 0.44 \quad (12)$$

The moment from the initial imperfection is also added in the minor axis, as indicated in the following equation

$$M_{z,imp}(x) = N_{Ed}e_{imp}k' \sin\left(\frac{\pi x}{L}\right) \quad (13)$$

Also, a moment magnification factor (k') which takes into account the second order effects needs to be taken into account. In this case, a parabolic bending moment distribution is considered, therefore $\beta = 1$ (from Table 6.4 in EN1994-1-1 (CEN 2004b)).

The value of the member imperfection (e_{imp}) is taken from Table 6.5 in EN1994-1-1, as a function of the percentage of reinforcement ($L/300$ for reinforcement ratios lower than 3% and $L/200$ for higher reinforcement ratios).

Finally, the resulting bending moments about major and minor axis, are respectively

$$M_{y,tot,Ed}(x) = M_{y,Ed}(x) \quad (14)$$

$$M_{z,tot,Ed}(x) = M_{z,Ed}(x) + M_{z,imp}(x) \quad (15)$$

Note that when superimposing the moment from imperfection to the moment from eccentricity, only in the case corresponding to $r = 1$ (constant bending moment) the critical section is located at mid-height of the column. For the rest of end moment ratios studied ($r = 0, -1$), the position of the critical section can be located by searching the maximum value of the bending moment in the above expressions.

Once the applied bending moments are calculated in both axes, a 3D plot of the points ($N_{Ed}, M_{z,Ed}, M_{y,Ed}$) from the parametric studies can be generated, as shown in Fig. 16.

Using the cross-sectional interaction curves at different load levels (i.e., horizontal cuts in Fig. 16) derived theoretically from the Matlab code (see Section 5.1), the three-dimensional interaction surface has been built-up, following a similar procedure to that described in (Bonet *et al.* 2004). The numerical points from the parametric studies carried out in ABAQUS are superimposed with the 3D interaction surface in Fig. 16, where the values of the axial load and bending moments on each axis have been divided by the cross-section plastic axial load and plastic bending moments, respectively. As it can be seen, all the points from the parametric studies lie outside the three-dimensional surface, meaning that EN1994-1-1 provides a conservative boundary for estimating the load-bearing capacity of CFST columns under biaxial bending. This boundary results overly conservative using exponents equal to one in Eq. (3) (straight line in the sectional interaction equation), while

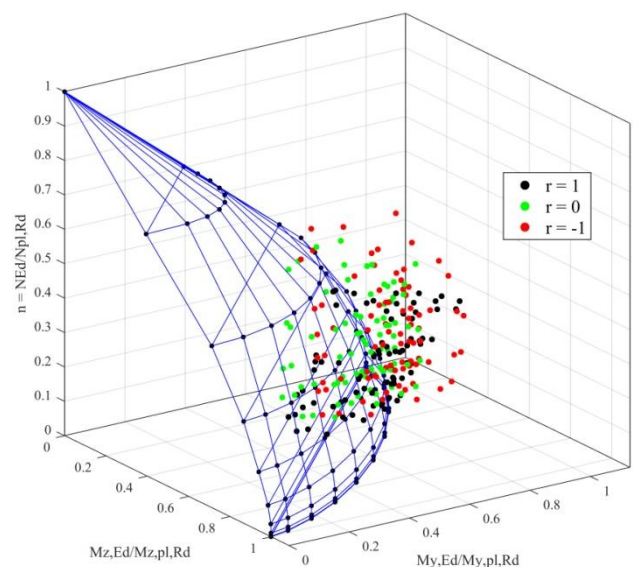


Fig. 16 Three-dimensional interaction surface and numerical results

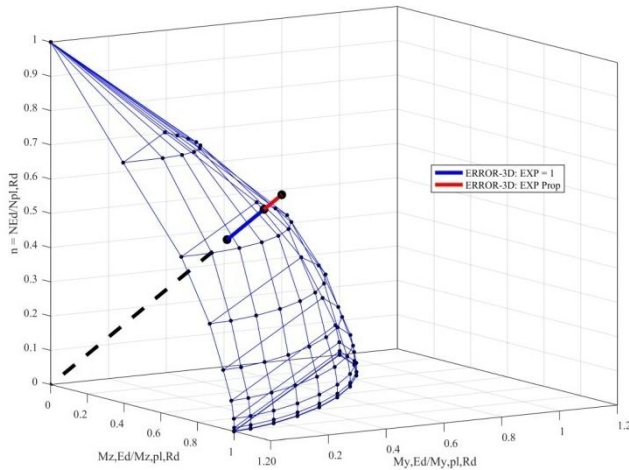


Fig. 17 Definition of the 3D error (ξ_{3D})

giving more reasonable results with the proposed exponents (Eq. (8)) and still lying on the safe side.

In order to get a measure of the error between the numerical results and the proposed interaction surface and being able to quantify the deviation of this interaction surface to the real behaviour of the columns, a 3D error has been defined. This error is obtained through a graphic procedure, as shown in Fig. 17 and explained below:

- (1) A straight line is plotted by linking the coordinates origin with the 3D numerical point
- (2) The intersection point between this line and the 3D interaction surface is obtained

The 3D error is then defined as the quotient between the module of the vectors measured from the coordinates origin to the numerical point and predicted point (intersection with 3D interaction surface), respectively.

$$\xi_{3D} = \frac{\left| (0,0,0) - \left(N / N_{pl}, M_y / M_{pl,y}, M_z / M_{pl,z} \right)_{NUM} \right|_n}{\left| (0,0,0) - \left(N / N_{pl}, M_y / M_{pl,y}, M_z / M_{pl,z} \right)_{PRED} \right|_n} \quad (16)$$

Following this procedure, the 3D error of the 240 cases simulated numerically with respect to the interaction surface has been measured. A summary of the prediction errors is given in Table 6. For each end moment ratio ($r = 1, 0, -1$), the average error and standard deviation are given under two cases: a) using the current approach from EN1994-1-1 (CEN 2004b) (exponents “a” and “b” equal to one) and b) using the proposed equation for the shape of the interaction surface.

The total 3D error (ξ_{3D}) and standard deviation is also given. As it can be seen, applying the current criterion in EC4 with a straight line results overly conservative with a mean value of 1.32 and standard deviation of 0.11, while the proposed equation gives much more accurate predictions, with an average value of the error of 1.10 and standard deviation of 0.09. By studying the different groups of end moment ratios, it can be seen that the proposed interaction surface results more accurate for constant bending moment ($r = 1$) with average error 1.08 (versus

Table 6 Summary of the 3D error (ξ_{3D}) from EC4 predictions and proposed equation

		Current EC4 (a = b = 1)	Proposed Eq. (8)
$r = 1$	Mean	1.29	1.08
	Std. dev.	0.09	0.08
$r = 0$	Mean	1.27	1.07
	Std. dev.	0.09	0.07
$r = -1$	Mean	1.39	1.17
	Std. dev.	0.11	0.08
All cases	Mean	1.32	1.10
	Std. dev.	0.11	0.09

1.29 from EC4) and end moment ratio $r = 0$, with average error 1.07 (versus 1.27 from EC4). For the case of end moment ratio $r = -1$ the average error of the proposal is 1.17, although it results conservative and more precise than the current approach in EC4, with average error 1.39 and more scattered predictions. This higher deviation of the predictions in the case of end moment ratio $r = -1$ may be related to the double curvature bending that occurs in this case, which makes the column “auto-compensate” the applied end moments and thus at its mid-section - where the maximum moment from imperfection is located - the first order bending moment is zero, therefore this situation is more favourable for the columns, i.e. the maximum bending moment is located at the column ends. This situation will be studied in more detail in future investigations, in order to develop a more accurate proposal for double curvature bending.

The distribution of the 3D error with the column slenderness (measured about minor axis) can be seen in Fig. 18 for the three groups of end moment ratios studied ($r = 1, 0, -1$). In these graphs, the errors obtained with the proposed equation are compared with those obtained by applying the current EN1994-1-1 (CEN 2004b) biaxial equation (exponents “a” and “b” equal to unity). It can be seen that the distribution of the error for the proposal is more uniform than that of the EC4 equation and less conservative, although with a safe average value. While in the EC4 equation most of the values lie above the +25% error, resulting overly conservative, with the proposed equation these errors are mostly confined between -10% and +25%, with a lower dispersion and average value closer to one. Again, it is observed that the proposal gives more conservative results for double curvature bending ($r = -1$), situation that will be studied in more detail in future research. Further experimental results are needed in order to generalize the presented work.

6. Conclusions

This work presented the results of a numerical investigation on the behaviour of slender CFST rectangular columns subjected to biaxial bending. A three-dimensional finite element model was fully described and validated by

comparison against experimental tests available in the consulted literature, obtaining reliable results. Different minor and major axis eccentricities as well as varying end moment ratios were included amongst the validation cases, covering uniaxial and biaxial bending and variable bending moment distributions.

By means of the validated numerical model, parametric studies were carried out on concrete-filled rectangular hollow section columns subjected to biaxial bending, with the aim of generating a numerical database that serves as a basis for the assessment of the current design guidelines of EN1994-1-1 for biaxial bending.

A total of 240 case analysis were generated, by combining the three different aspect ratios, five member slenderness and 16 loading positions with eccentricities about both minor and major axes. The influence of the main parameters over the column capacity in biaxial bending was studied, showing that for increasing eccentricities the ultimate load progressively decreased. It was also observed that the situations with variable bending moment distribution, especially end moment ratio $r = -1$, were more favourable for the columns than applying a constant bending moment distribution - i.e., end moment ratio $r = 1$ -. The member slenderness showed a negative influence over the column capacity under biaxial bending, reducing the column capacity with increasing slenderness values.

For the cases analysed, the three-dimensional $M-N$ interaction surface was built up with the help of a computer algorithm developed by the authors in Matlab. The numerical points obtained from the parametric studies were compared with the computed interaction surface, and the 3D error was measured with a graphic procedure. A new shape of the interaction curve in EN1994-1-1 using exponents different to unity was proposed by the authors through a simple equation, which lies between the current interaction curves used in the Eurocodes for steel (EC3) and concrete (EC2). The comparison of the errors showed that the current criterion in EN1994-1-1 results overly conservative, while the interaction curve proposed by the authors provides more accurate results, still lying on the safe side. It was also observed that the results for columns with end moment ratio $r = -1$ are more conservative both in the proposal and current EN1994-1-1 method, indicating that for double curvature bending further studies and experimental results would be needed.

Acknowledgments

The authors gratefully acknowledge “Conselleria d’Educació, Investigació, Cultura i Esport” of the Valencian Community (Spain) for funding the project GV/2017/026.

The authors would also like to thank Leibniz Universität Hannover for providing the financial support of the research stay of Maximilian Mund at Universitat Politècnica de València.

References

- ABAQUS (2014), Abaqus/Standard Version 6.14 User’s Manual: Volumes I-III; Pawtucket, Rhode Island: Hibbit, Karlsson & Sorensen, Inc.
- Albero, V., Espinos, A., Romero, M.L., Hospitaler, A., Bihina, G. and Renaud, C. (2016), “Proposal of a new method in EN1994-1-2 for the fire design of concrete-filled steel tubular columns”, *Eng. Struct.*, **128**, 237-255.
<https://doi.org/10.1016/j.engstruct.2016.09.037>
- Anderson, D. (1992), “Calibration of composite columns: Eurocode 4 and British practice”, Report to Building Research Establishment. Department of Environment.
- Bonet, J.L., Miguel, P.F., Fernandez, M.A. and Romero, M.L. (2004), “Analytical approach to failure surfaces in reinforced concrete sections subjected to axial loads and biaxial bending”, *J. Struct. Eng.*, **130**(12), 2006-2015.
[https://doi.org/10.1061/\(ASCE\)0733-9445\(2004\)130:12\(2006\)](https://doi.org/10.1061/(ASCE)0733-9445(2004)130:12(2006))
- Bresler, B. (1960), “Design criteria for reinforced columns under axial load and biaxial bending”, *J. Am. Concrete Inst.*, **32**(5), 481-490.
- CEN (2004a), EN 1992-1-1, Eurocode 2: Design of concrete structures. Part 1-1: General rules and rules for buildings, Comité Européen de Normalisation, Brussels, Belgium.
- CEN (2004b), EN 1994-1-1, Eurocode 4: Design of composite steel and concrete structures. Part 1-1: General rules and rules for buildings, Comité Européen de Normalisation, Brussels, Belgium.
- CEN (2005), EN 1993-1-1, Eurocode 3: Design steel structures. Part 1-1: General rules and rules for buildings, Comité Européen de Normalisation, Brussels, Belgium.
- Dundar, C. and Tokgoz, S. (2012), “Strength of biaxially loaded high strength reinforced concrete columns”, *Struct. Eng. Mech., Int. J.*, **44**(5), 649-661.
<https://doi.org/10.12989/sem.2012.44.5.649>
- Dundar, C., Tokgoz, S., Tanrikulu, A.K. and Baran, T. (2008), “Behaviour of reinforced and concrete-encased composite columns subjected to biaxial bending and axial load”, *Buildi. Environ.*, **43**(6), 1109-1120.
<https://doi.org/10.1016/j.buildenv.2007.02.010>
- Espinos, A., Romero, M.L. and Hospitaler, A. (2010), “Advanced model for predicting the fire response of concrete filled tubular columns”, *J. Constr. Steel Res.*, **66**(8-9), 1030-1046.
<https://doi.org/10.1016/j.jcsr.2010.03.002>
- Espinós, A., Albero, V., Romero, M.L., Mund, M., Kleiboemer, I., Meyer, P. and Schaumann, P. (2018), “Numerical investigation on slender concrete-filled steel tubular columns subjected to biaxial bending”, *Proceedings of the 12th International Conference on Advances in Steel-Concrete Composite Structures (ASCCS 2018)*, Valencia, Spain.
- FIB (2010), Model Code 2010 (Volume 1), FIB, Lausanne, Switzerland.
- Goode, C.D. and Lam, D. (2008), “Concrete-filled steel tube columns— Test compared with Eurocode 4”, *Composite Construction VI*, Devil’s Thumb Ranch, CO, USA, July.
- Guo, L.H., Wang, Y.Y. and Zhang, S.M. (2012), “Experimental study of concrete-filled rectangular HSS columns subjected to biaxial bending”, *Adv. Struct. Eng.*, **15**(8), 1329-1344.
<https://doi.org/10.1260/1369-4332.15.8.1329>
- Han, L.-H., Li, W. and Bjorhovde, R. (2014), “Developments and advanced applications of concrete-filled steel tubular (CFST) structures: Members”, *J. Constr. Steel Res.*, **100**, 211-228.
<https://doi.org/10.1016/j.jcsr.2014.04.016>
- Hernández-Figueirido, D., Romero, M.L., Bonet, J.L. and Montalvá, J.M. (2012a), “Ultimate capacity of rectangular concrete-filled steel tubular columns under unequal load eccentricities”, *J. Constr. Steel Res.*, **68**(1), 107-117.

- <https://doi.org/10.1016/j.jcsr.2011.07.014>
- Hernández-Figueirido, D., Romero, M.L., Bonet, J.L. and Montalvá, J.M. (2012b), "Influence of slenderness on high-strength rectangular concrete-filled tubular columns with axial load and nonconstant bending moment", *J. Struct. Eng.*, **138**(12), 1436-1445.
- [https://doi.org/10.1061/\(ASCE\)ST.1943-541X.0000590](https://doi.org/10.1061/(ASCE)ST.1943-541X.0000590)
- Leite, L.C., Bonet, J.L., Pallarés, L. and Miguel, P.F. (2014), "Cm-factor for RC slender columns under unequal eccentricities and skew angle loads at the ends", *Eng. Struct.*, **71**, 73-87.
- <https://doi.org/10.1016/j.engstruct.2014.04.020>
- Leon, R.T., Perea, T., Hajjar, J.F. and Denavit, M.D. (2011), *Concrete-filled tubes columns and beam-columns: a database for the AISC 2005 and 2010 specifications*, Institute für Konstruktiven Ingenieurbau (IKIB), Bergische Universität Wuppertal, Wuppertal, Germany.
- Li, G., Yang, Z., Lang, Y. and Fang, C. (2016), "Behavior of CFST columns with inner CFRP tube under biaxial eccentric loading", *Steel Compos. Struct., Int. J.*, **22**(6), 1487-1505.
- <https://doi.org/10.12989/scs.2016.22.6.1487>
- Liang, Q.Q. (2008), "Nonlinear analysis of short concrete-filled steel tubular beam-columns under axial load and biaxial bending", *J. Constr. Steel Res.*, **64**(3), 295-304.
- <https://doi.org/10.1016/j.jcsr.2007.07.001>
- Liang, Q.Q. (2015), *Analysis and Design of Steel and Composite Structures*, CRC Press, Taylor & Francis Group, Boca Raton, FL, USA.
- Liang, Q.Q., Patel, V.I. and Hadi, M.N.S. (2012), "Biaxially loaded high-strength concrete-filled steel tubular slender beam-columns, Part I: Multiscale simulation", *J. Constr. Steel Res.*, **75**, 64-71. <https://doi.org/10.1016/j.jcsr.2012.03.005>
- MathWorks (2016), *MATLAB*, Natick, Massachusetts USA.
- Matsui, C., Tsuda, K. and Ishibashi, Y. (1995), "Slender concrete filled steel tubular columns under combined compression and bending", *Proceedings of the 4th Pacific Structural Steel Conference*, Singapore.
- O'Shea, M.D. and Bridge, R.Q. (2000), "Design of circular thin-walled concrete filled steel tubes", *J. Struct. Eng.*, **126**(11), 1295-1303.
- [https://doi.org/10.1061/\(ASCE\)0733-9445\(2000\)126:11\(1295\)](https://doi.org/10.1061/(ASCE)0733-9445(2000)126:11(1295))
- Patel, V.I., Liang, Q.Q. and Hadi, M.N.S. (2012a), "High strength thin-walled rectangular concrete-filled steel tubular slender beam-columns, Part I: Modeling", *J. Constr. Steel Res.*, **70**, 377-384. <https://doi.org/10.1016/j.jcsr.2011.10.019>
- Patel, V.I., Liang, Q.Q. and Hadi, M.N.S. (2012b), "High strength thin-walled rectangular concrete-filled steel tubular slender beam-columns, Part II: Behavior", *J. Constr. Steel Res.*, **70**, 368-376. <https://doi.org/10.1016/j.jcsr.2011.10.021>
- Patel, V.I., Liang, Q.Q. and Hadi, M.N.S. (2014), "Behavior of biaxially-loaded rectangular concrete-filled steel tubular slender beam-columns with preload effects", *Thin-Wall. Struct.*, **79**, 166-177. <https://doi.org/10.1016/j.tws.2014.02.013>
- Patel, V.I., Liang, Q.Q. and Hadi, M.N.S. (2015), "Biaxially loaded high-strength concrete-filled steel tubular slender beam-columns, part II: Parametric study", *J. Constr. Steel Res.*, **110**, 200-207. <https://doi.org/10.1016/j.jcsr.2012.03.029>
- Patel, V.I., Liang, Q.Q. and Hadi, M.N.S. (2017), "Nonlinear analysis of biaxially loaded rectangular concrete-filled stainless steel tubular slender beam-columns", *Eng. Struct.*, **140**, 120-133. <https://doi.org/10.1016/j.engstruct.2017.02.071>
- Perea, T., Leon, R.T., Hajjar, J.F. and Denavit, M.D. (2013), "Full-scale tests of slender concrete-filled tubes: axial behavior", *J. Struct. Eng.*, **139**(7), 1249-1262.
- [https://doi.org/10.1061/\(ASCE\)ST.1943-541X.0000784](https://doi.org/10.1061/(ASCE)ST.1943-541X.0000784)
- Perea, T., Leon, R.T., Hajjar, J.F. and Denavit, M.D. (2014), "Full-scale tests of slender concrete-filled tubes: Interaction behavior", *J. Struct. Eng.*, **140**(9), 04014054.
- [https://doi.org/10.1061/\(ASCE\)ST.1943-541X.0000949](https://doi.org/10.1061/(ASCE)ST.1943-541X.0000949)
- Tokgoz, S. and Dundar, C. (2008), "Experimental tests on biaxially loaded concrete-encased composite columns", *Steel Compos. Struct., Int. J.*, **8**(5), 423-438.
- <https://doi.org/10.12989/scs.2008.8.5.423>
- Tokgoz, S. and Dundar, C. (2010), "Experimental study on steel tubular columns in-filled with plain and steel fiber reinforced concrete", *Thin-Wall. Struct.*, **48**(6), 414-422.
- <https://doi.org/10.1016/j.tws.2010.01.009>
- Tokgoz, S., Dundar, C. and Tanrikulu, A.K. (2012), "Experimental behaviour of steel fiber high strength reinforced concrete and composite columns", *J. Constr. Steel Res.*, **74**, 98-107.
- <https://doi.org/10.1016/j.jcsr.2012.02.017>
- Wang, Y.C. (1999), "Tests on slender composite columns", *J. Constr. Steel Res.*, **49**(1), 25-41.
- [https://doi.org/10.1016/S0143-974X\(98\)00202-8](https://doi.org/10.1016/S0143-974X(98)00202-8)
- Zhao, G.T., Zhang, M.X. and Li, Y.H. (2009), "Behavior of slender steel concrete composite columns in eccentric loading", *J. Shanghai Univ. (English Edition)*, **13**(6), 481.
- <https://doi.org/10.1007/s11741-009-0611-2>

DL